Materials International
Open-Access Journal (ISSN: 2668-5728)

Article
Volume 7, Issue 4, 2025, 32
https://doi.org/10.33263/Materials74.032

Increasing Gas Adsorption Sensitivity of Ternary AlGaN Alloy through AlGaXN (X=Si, Ge, Pd, Pt) Nanoarchitectures: A First Principles Study

Fatemeh Mollaamin [1,*]

[1] Department of Biomedical Engineering, Faculty of Engineering and Architecture, Kastamonu University, Kastamonu, Turkey
* Correspondence: fmollaamin@kastamonu.edu.tr;

Received: 15.02.2025; Accepted: 29.07.2025; Published: 10.12.2025

Abstract: This article investigates hydrogen grabbing towards the formation of hetero-clusters of H@AlGaN, H@AlGaSiN, H@AlGaGeN, H@AlGaPdN, and H@AlGaPtN was carried out using DFT computations at the CAM–B3LYP–D3/6-311+G (d,p) level of theory. The notable decrease in signal intensity near the parallel edge of the nanocluster sample might be due to silicon or germanium binding, or to an induced non-spherical distribution of AlGaSiN or AlGaGeN heteroclusters. However, there is a significant deviation from using palladium or platinum as electron acceptors on the surfaces of AlGaPdN or AlGaPtN heteroclusters. The hypothesis of the energy-adsorption phenomenon was confirmed by the density distributions of CDD, DOS/PDOS, and ESP for AlGaN and its alloys. Therefore, it can be considered that palladium or platinum atoms in the functionalized AlGaPdN or AlGaPtN might have more impressive sensitivity for accepting the electrons in the process of hydrogen adsorption. Furthermore, AlGaPdN or AlGaPtN may be advantageous for certain high-frequency applications that require solar cells for energy storage. The advantages of platinum or palladium over aluminum gallium nitride include higher electron and hole mobilities, enabling platinum- or palladium-doped devices to operate at higher frequencies than silicon- or germanium-doped devices. As a matter of fact, it can be observed that doped heteroclusters of AlGaPdN or AlGaPtN might ameliorate the capability of AlGaN in transistor cells for energy storage. In fact, the study of Si-/Ge-/Pd-/Pt-doped AlGaN hetero-cluster shows promise for a high-performance electronic device and hydrogen gas sensing applications.

Keywords: hydrogen adsorption; energy storage; transistor cells; aluminum gallium nitride; silicon; germanium; palladium; platinum.

1. Introduction

The surface and microstructure of the sensitive material play an important role in gas adsorption and detection. A binary III/V direct-bandgap semiconductor called Gallium nitride (GaN) is a very hard material with a wide bandgap and is applied in a variety of technologies, including optoelectronics, high-power electronics, and light-emitting diodes, partly due to its favorable thermal properties.

The nitrides of group III in the periodic table are relatively insensitive to ionizing radiation, making them suitable materials for solar cell arrays on satellites. Therefore, space applications could also benefit, as devices have shown stability in high-radiation environments [1–7].

Ternary "AlGaN" alloys have been recognized as promising materials for realizing deep ultraviolet "DUV" optoelectronic devices with operating wavelengths down to 200 nm. For the development of high-performance AlGaN-based "DUV" devices, high-conductivity p-type Al-rich $Al_xGa_{1-x}N$ ($x \geq 0.4$) is essential. Many studies have shown that enhancing the p-type conductivity has a significant effect on the improvement of both the electrical and optical properties of AlGaN DUV optoelectronics [8–15].

The influence of two different methods of silicon doping in "AlGaN" layer, that is, modulation-doping "MD" and delta-doping "DD", on the optical and electrical performance of deep ultraviolet light-emitting diodes "DUV-LEDs" has been investigated. Both the photoluminescence and electroluminescence intensities in the "Si-DD" structure are stronger than those obtained by the "Si-MD" method, while the forward voltage and reverse leakage current are slightly smaller in the "DD" structure than those in the "MD" structure. Compared with the "MD" structure, the "DD" structure shows higher capacitance-voltage characteristics. This study suggests that the "DD" method can improve the optical and electrical performance of "DUV-LEDs" [16–25].

This study explores the impact of Si doping on the material properties of high-temperature annealed (HTA) $Al_{0.71}Ga_{0.29}N$ layers, which are grown on AlN/sapphire templates [26,27].

In this paper, we propose a feasible ternary semiconductor of aluminum gallium nitride, which is doped with silicon, germanium, palladium, or platinum. We carried out molecular modeling to examine the geometrical parameters of doping atoms on the surface of AlGaN, and we studied the absorption status and charge density of the solar cells. Moreover, the effect of a relative chemical shift between AlGaN and doped heteroclusters of the transistor cell was also investigated.

2. Materials and Methods

The Si-, Ge-, Pd-, or Pt-doped AlGaN nanocage was calculated within the framework of first-principles calculation based on density functional theory (DFT) [28–34] (Figure 1a–e, a′–e′). The rigid potential energy surface using density functional theory [35–42] was performed using the Gaussian 16 revision C.01 program package [43] and GaussView 6.1 [44]. The coordination input for energy storage on the solar cells has applied 6-311+G (d,p) and EPR–3 basis sets.

Figure 1 shows the process of energy storage on heteroclusters of AlGaN, AlGaSiN, AlGaGeN, AlGaPdN, or AlGaPtN, which are varied to maximize the absorption in the active region. Further, we optimized the structural parameters of the nanocluster of AlGaN, which is doped with silicon, germanium, palladium, and platinum, towards the formation of heteroclusters of AlGaSiN, AlGaGeN, AlGaPdN, and AlGaPtN for obtaining the highest short-circuit current density.

This is a utility used to calculate ring area and perimeter, since ring area is sometimes involved in wavefunction analysis. In this function, it is needed to input the index of the atoms in the ring in a clockwise manner, including Al5, Si5, Ge5, Pd5, Pt5, N4, Ga15, N7, Ga6, N12

(Figure 1a–e, a′–e′). Then, the total ring area and total ring perimeter for a tailored ring are 9.6981Å^2 and 11.6921 Å^2, respectively (Figure 1a–e, a′–e′).

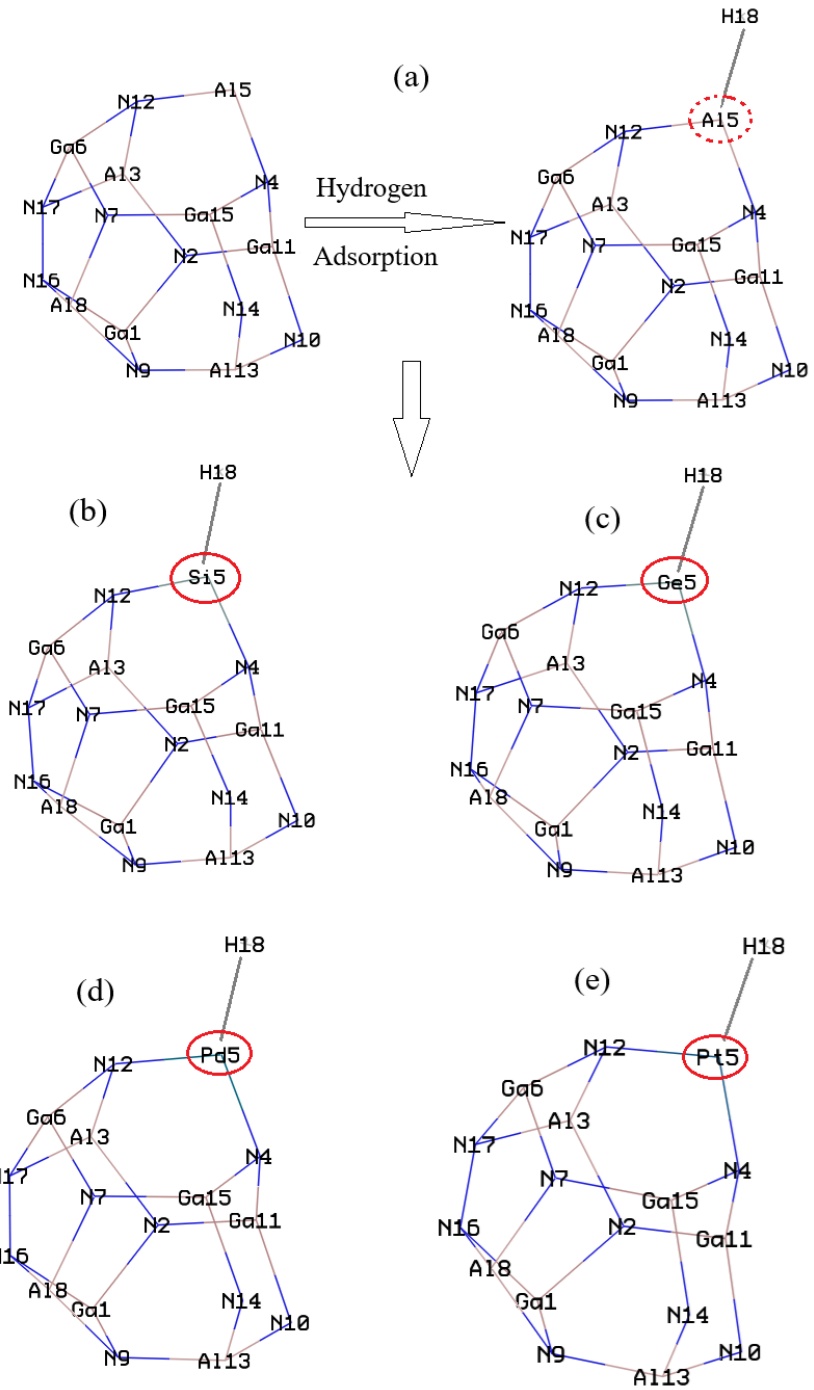

Figure 1. Characterization of hydrogenated nanohybrids of AlGaN, AlGaSiN, AlGaGeN, AlGaPdN, and AlGaPtN.

Since the DFT method is used for computational chemistry, the hybrid functional Becke 3-parameter Lee–Yang–Parr (B3LYP) [45] appears to offer the greatest contribution. A new hybrid exchange–correlation functional named the Coulomb-Attenuating Method with B3LYP (CAM–B3LYP) is proposed, which combines the hybrid qualities of B3LYP and the long-range correction [46].

Additionally, in the DFT–D3 method of Grimme et al., the following expression for the van der Waals (vdW) dispersion energy-correction term is used [47]:

$$E_{\text{disp}} = -\frac{1}{2}\sum_{i=1}^{N_{at}}\sum_{j=1}^{N_{at}}\sum_{L}\left(f_{d,6}\left(r_{ij,L}\right)\frac{C_{6ij}}{r_{ij,L}^{6}} + f_{d,8}\left(r_{ij,L}\right)\frac{C_{8ij}}{r_{ij,L}^{8}}\right) \quad (1)$$

The dispersion coefficients C_{6ij} are geometry dependent, as they are adjusted based on the local geometry (coordination number) around atoms *i* and *j*. Additionally, Electron Paramagnetic Resonance (EPR) has been performed, which is a method for studying materials with unpaired electrons. The basic concepts of EPR are analogous to those of NMR, but the spins excited are those of the electrons instead of the atomic nuclei [48]. Therefore, in our research, the calculations have been performed based on a CAM–B3LYP–D3/EPR–3 level of theory.

3. Results and Discussion

Si, Ge, Pd, and Pt are highly sensitive and selective materials for detecting H_2, and they have been widely used for H_2 detection. H_2 molecules can be adsorbed on the surface of Pd, and signals are transmitted through electron transfer on the surface. In this article, the data evaluate the efficiency of heteroclusters of AlGaN, AlGaSiN, AlGaGeN, AlGaPdN, and AlGaPtN for adsorption and storage energy in transistors.

3.1. Analysis of CDD, DOS/PDOS, and ESP.

The amounts of charge density differences, "CDD," are measured by considering isolated atoms or noninteracting ones. The mentioned approximation can be the lightest to use because the superposition value may be received from the primary status of the self-consistency cycle in the code that carries out the density functional theory (Figure 2a–e, a′–e′) [49,50].

In Figure 2a, a′ the atoms of Al5, H18 accompanying nitrogen and gallium atoms from AlGaN and H@AlGaN, respectively, have shown the fluctuation around –9 to +3 Bohr. The atoms of Si5, H18 accompanying aluminum, gallium, and nitrogen from AlGaSiN / H@AlGaSiN, respectively, have indicated the fluctuation around –9 to + 3 Bohr (Figure 2b,b′). However, the atoms of Ge5, H18 accompanying aluminum, gallium, and nitrogen from AlGaGeN and H@AlGaGeN have indicated the fluctuation around –9 to + 5 Bohr and –9 to + 7 Bohr, respectively (Figure 2c,c′). For two nanoclusters of AlGaPdN (Figure 2d,d′) and AlGaPtN (Figure 2e,e′), it was observed that the fluctuation around –9 to –1 Bohr for aluminum, gallium, and nitrogen and Pd5 or Pt5 and H18 before H-adsorption and between –9 to +6 Bohr after H-adsorption.

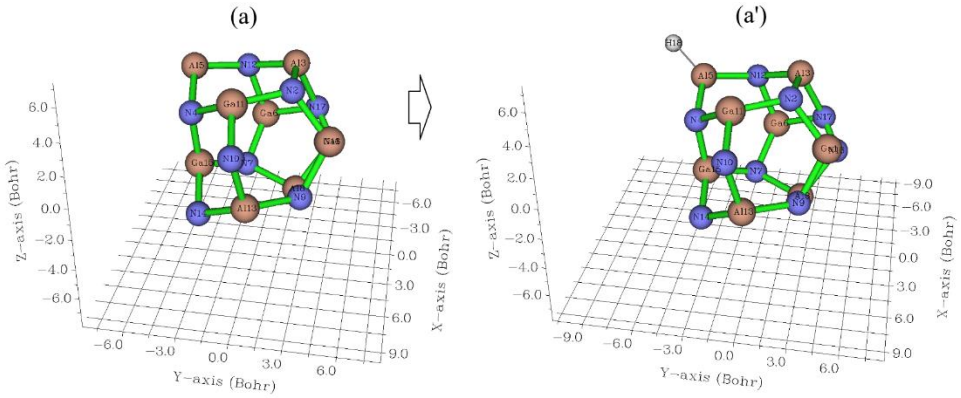

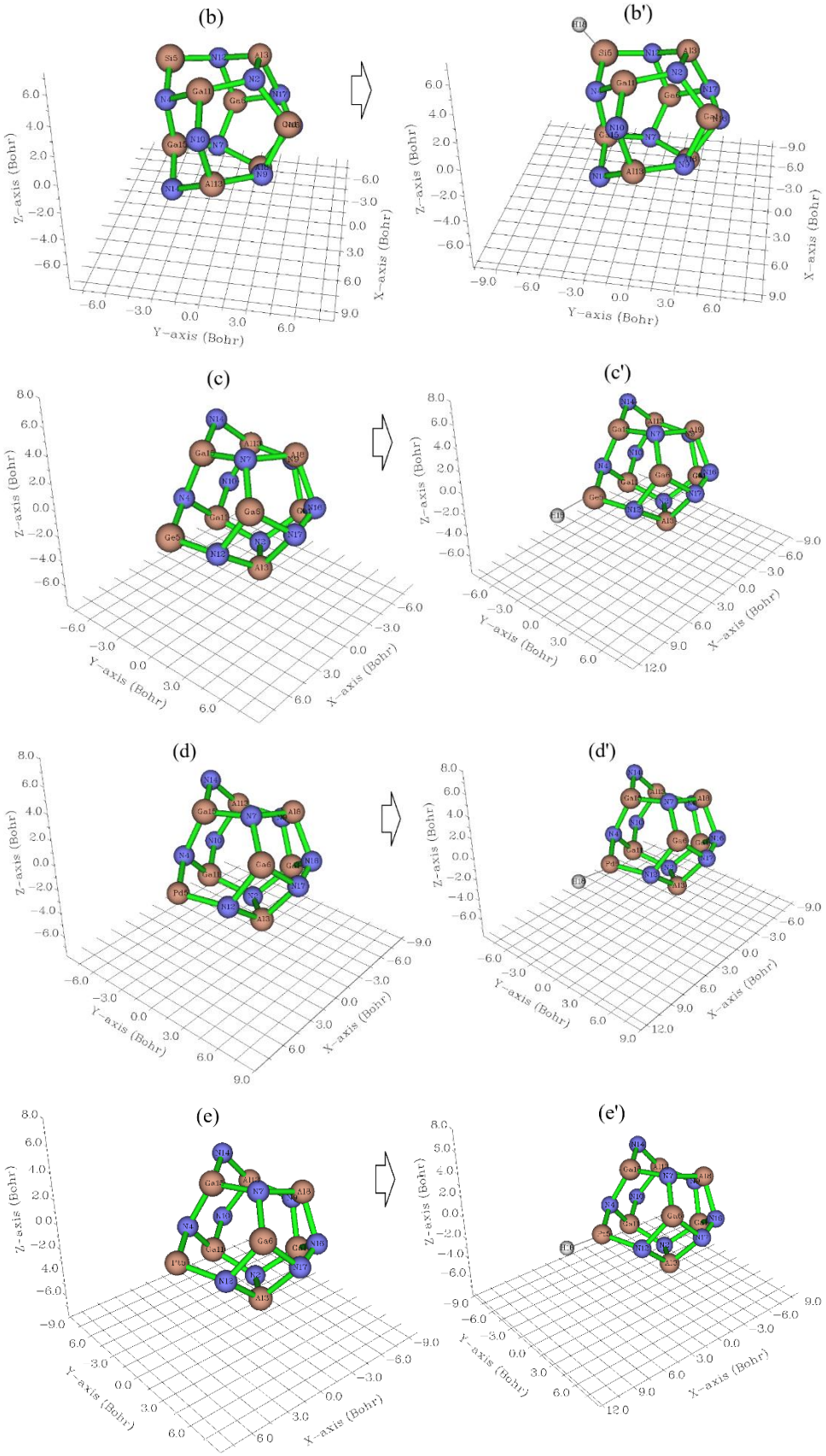

Figure 2. CDD graphs for hetero-clusters through hydrogen adsorption, including **(a)** AlGaN; **(a′)** H@AlGaN; **(b)** AlGaSiN; **(b′)** H@AlGaSiN; **(c)** AlGaGeN; **(c′)** H@AlGaGeN; **(d)** AlGaPdN; **(d′)** H@AlGaPdN; **(e)** AlGaPtN; **(e′)** H@AlGaPtN.

Density of states (DOS) is an important concept of solid physics, which represents the number of states in a unit energy interval, since energy levels are contiguous, so that DOS can be plotted as a curve map. In an isolated system (such as a molecule), the energy levels are discrete, and the concept of DOS is questionable; some people argue that DOS is completely valueless in this situation. However, if the discrete energy levels are broadened artificially to curve artificially, the DOS graph can be used as a valuable tool for analyzing the nature of electron structure. In an isolated system, the energy levels are discrete; the concept of the density of states (DOS) is therefore completely valueless in this situation. In the negative part, the region between –5 to –12 a.u. has obviously larger state density than other regions for AlGaN/ H@AlGaN (Figure 3a,a′), (b) AlGaSiN/H@AlGaSiN(Figure 3b,b′), AlGaGeN/ H@AlGaGeN (Figure 3c,c′), AlGaPdN/ H@AlGaPdN (Figure 3d,d′), and (e) AlGaPtN/ H@AlGaPtN(Figure 3e,e′). It is remarkable that the excessive growth technique of doping silicon, germanium, palladium, and platinum into an aluminum gallium nitride alloy is a potential approach to designing high-efficiency hybrid semipolar derivatives in the long-wavelength region.

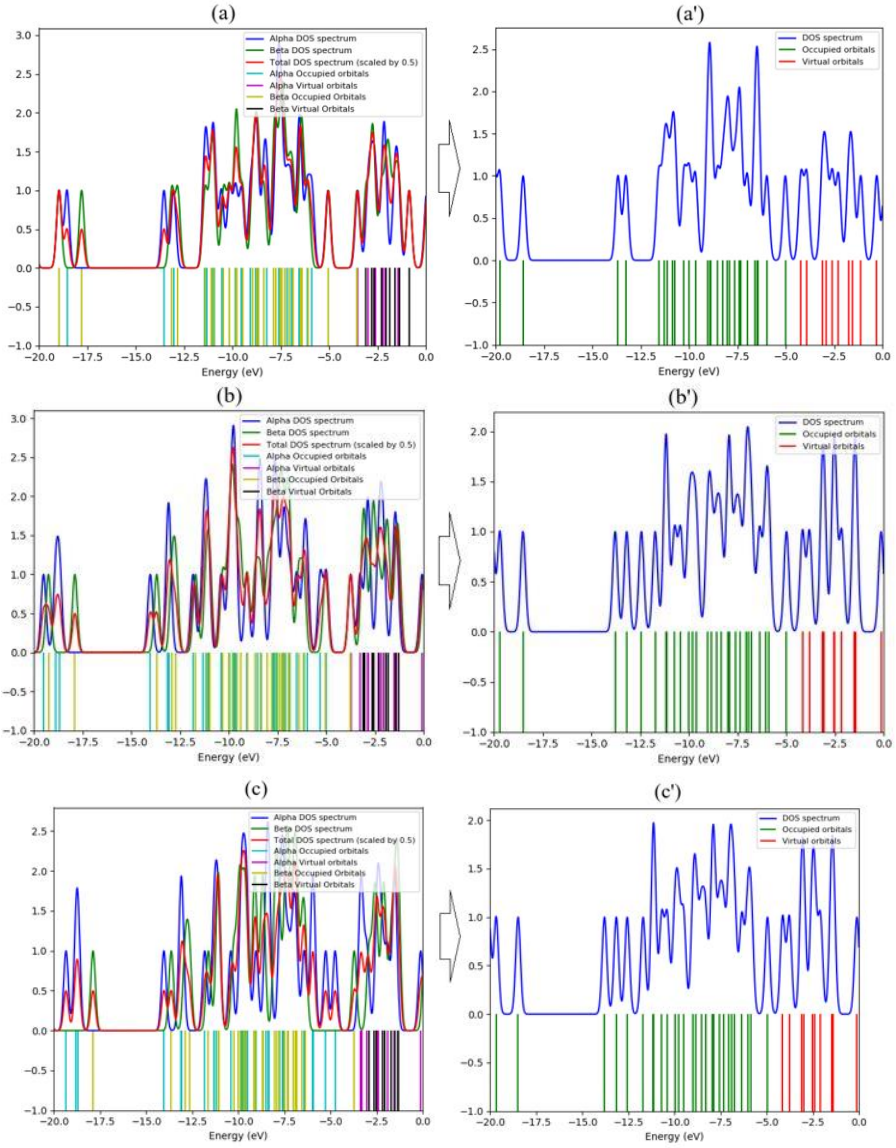

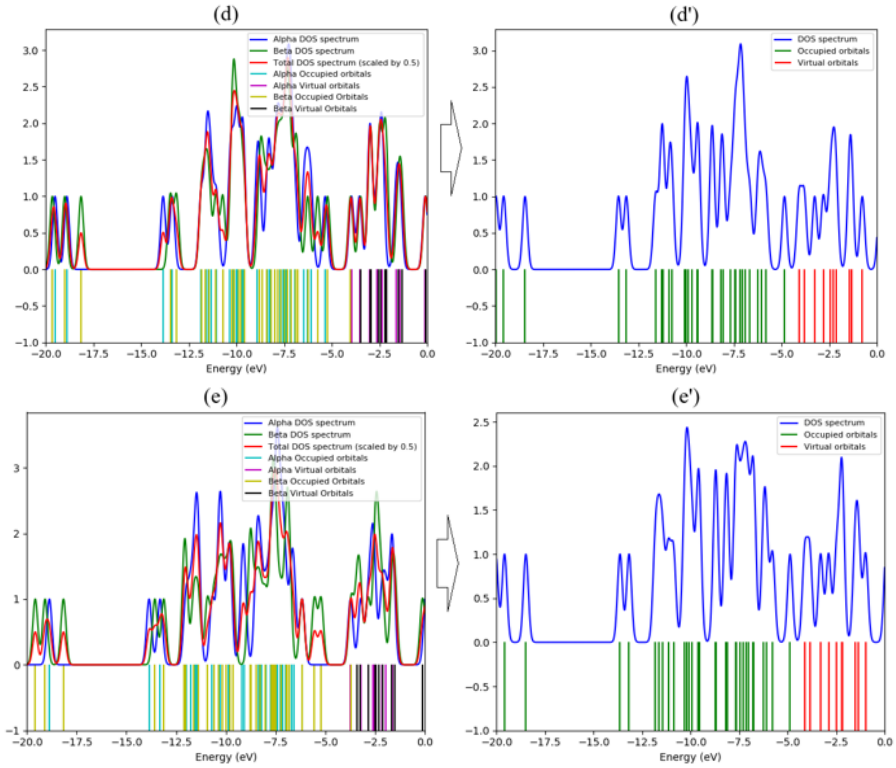

Figure 3. DOS graphs of heteroclusters include **(a)** AlGaN; **(a′)** H@AlGaN; **(b)** AlGaSiN; **(b′)** H@AlGaSiN; **(c)** AlGaGeN; **(c′)** H@AlGaGeN; **(d)** AlGaPdN; **(d′)** H@AlGaPdN; **(e)** AlGaPtN; **(e′)** H@AlGaPtN.

ESP or Molecular electrostatic potential was broadly exploited to predict the nucleophilic and electrophilic zones for a long time. It is also noteworthy for pursuing H-bonds, halogen bonds, molecular recognition, and intermolecular interactions involving aromatic structures. [51–54].

$$V_{tot}(r) = V_{nuc}(r) + V_{ele}(r) = \sum_A \frac{Z_A}{|r-R_A|} - \int \frac{\rho(r')}{|r-r'|} dr' \qquad (2)$$

Z_A is the nuclear charge; if a pseudopotential is used, then Z_A is the number of explicitly expressed electrons.

The compounds of H@AlGaN, H@AlGaSiN, H@AlGaGeN, H@AlGaPdN, and H@AlGaPtN can be defined by ESP graphs owing to exploring their delocalization/localization characterizations of electrons and chemical bonds (Figure 4a–e).

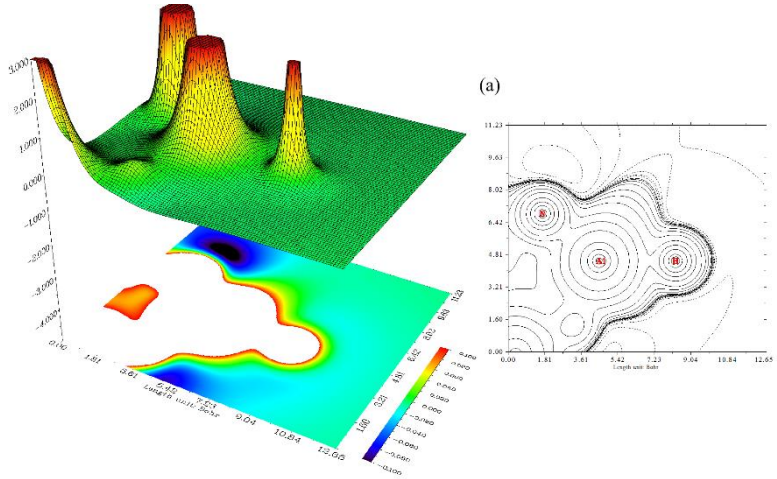

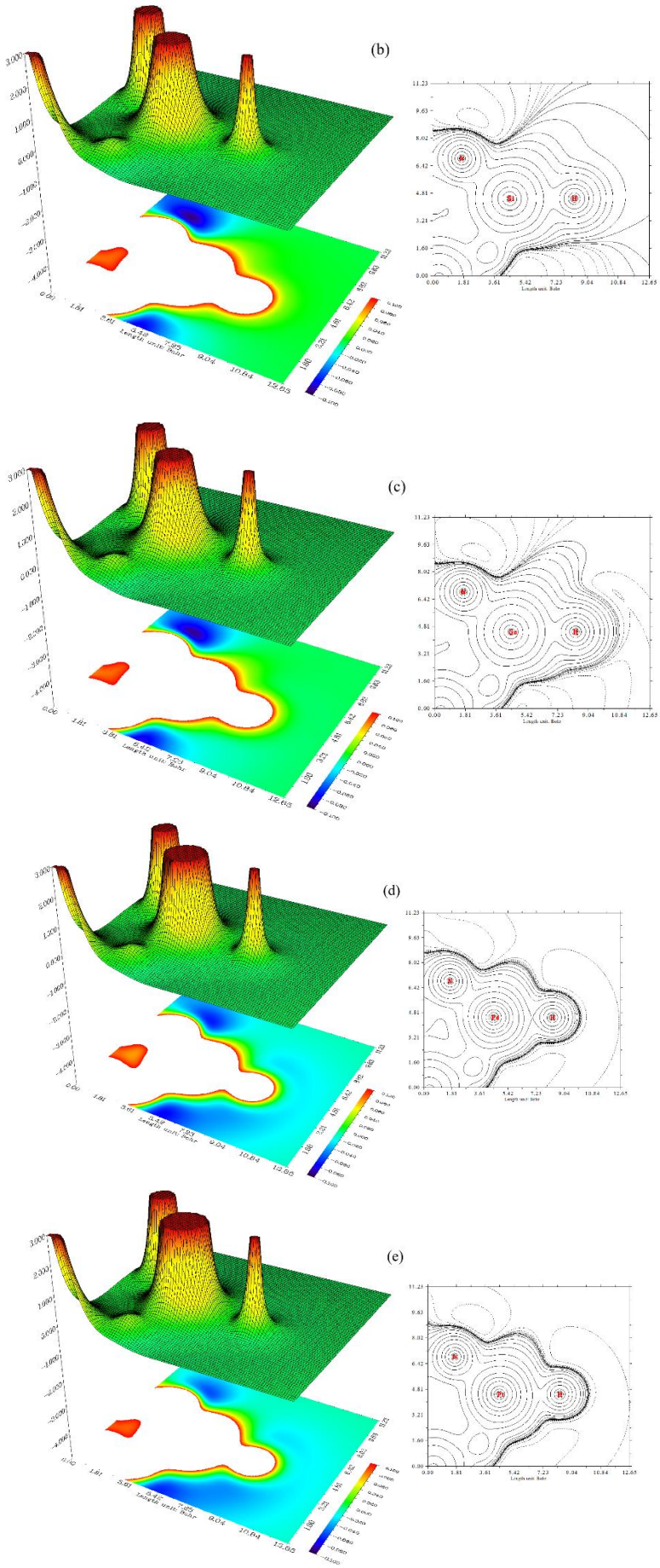

Figure 4. The graphs of ESP for hetero-clusters include **(a)** H@AlGaN; **(b)** H@AlGaSiN; **(c)** H@AlGaGeN; **(d)** H@AlGaPdN; **(e)** H@AlGaPtN. (Counter line map on the right and shaded surface map with projection on the left)

The counter map of ESP for H@AlGaN has shown the electron delocalization due to labeling atoms of N(4), Al (5), and H (18) (Figure 4a). Then, hydration of Si- and Ge-doped AlGaN indicates a larger isosurface map of electron delocalization due to labeling atoms of N(4), Si (5), H (18) of AlGaSiN –H (Figure 4b) and N(4), Ge (5), H (18) of H@AlGaGeN (Figure 4c). A vaster jointed area engaged by an isosurface map for Pd and Pt doping AlGaN towards formation of hetero-clusters of H@AlGaPdN (Figure 4d) and H@AlGaPtN (Figure 4e) after hydrogen adsorption due to labeling atoms of N(4), Pd/Pt(5), H (18), respectively. A smaller connected area in an isosurface map indicates that electron delocalization is relatively difficult. However, the large counter map of ESP for H@AlGaPtN, H@AlGaPdN, H@AlGaSiN, and H@AlGaGeN can confirm that doping Pd, Pt, Si, and Ge nanoparticles on the surface increases the efficiency of the ternary transistor cell of AlGaN for energy storage. Besides, the changes of charge density analysis have illustrated that pure AlGaN has shown the Bader charge of –1.272 coulomb, and after doping with silicon, germanium, palladium, and platinum, it has indicated the Bader charge of –1.290, –1.285, –1.292, –1.309 coulomb for hybrid composites of AlGaSiN, AlGaGeN, AlGaPdN, AlGaPtN, respectively, that describes the tensity value of these hetero-clusters for energy storage.

Moreover, the intermolecular orbital overlap integral is important in discussions of intermolecular charge transfer, which can calculate HOMO-HOMO and LUMO-LUMO overlap integrals between the hydrogen atom and hybrid hetero-clusters of AlGaN, AlGaSiN, AlGaGeN, AlGaPdN, and AlGaPtN. The wavefunction level we used is CAM–B3LYP–D3/6-311+G(*d*, *p*) that corresponds to HOMO and LUMO, respectively (Table 1).

Table1. LUMO/HOMO, energy gap (ΔE), and overlap integral for H@AlGaN, H@AlGaSiN, H@AlGaGeN, H@AlGaPdN, H@AlGaPtN.

Hetero-clusters	E_{LUMO} (a.u.)	E_{HOMO} (a.u.)	$\Delta E=E_{LUMO}-E_{HOMO}$ (a.u.)	$< S^2 >$
H@AlGaN	–0.1550	–0.1846	0.0296	1.7500
H@AlGaSiN	–0.1531	–0.1833	0.0302	2.0022
H@AlGaGeN	–0.1519	–0.1822	0.0303	2.6557
H@AlGaPdN	–0.1499	–0.1780	0.0281	2.6260
H@AlGaPtN	–0.1513	–0.1791	0.0278	2.6349

For unrestricted wavefunctions, the orthonormalization condition does not hold in general between alpha and beta orbitals. This function computes the overlap matrix between alpha and beta orbitals:

$$S_{i,j}^{\alpha,\beta} = \int \varphi_i^{\alpha}(r)\varphi_j^{\beta}(r)dr \qquad (3)$$

The diagonal elements are useful for evaluating the matching degree of corresponding spin orbital pairs; an evident deviation from 1 indicates that spin polarization is remarkable. Because the expectation of the S^2 operator for a single determinant (SD) wavefunction can be easily derived from the matrix, Multiwfn [55–56] outputs this quantity together:

$$< S^2 >_{SD} = < S^2 >_{Exact} + N^{\beta} - \sum_i^{N^{\alpha}} \sum_j^{N^{\beta}} \left| S_{i,j}^{\alpha,\beta} \right|^2 \qquad (4)$$

where $< S^2 >_{Exact}$ is the exact value of the square of the total spin angular momentum:

$$< S^2 >_{Exact} = \frac{N^{\alpha}-N^{\beta}}{2}\left(\frac{N^{\alpha}-N^{\beta}}{2}+1\right) \qquad (5)$$

A strategy for increasing the square of an overlap integral ($< S^2 >$) of electrons in AlGaN is proposed by doping with Si, Ge, Pd, or Pt (Table 1). Therefore, E_{LUMO} (a.u.), E_{LUMO} (a.u.), and the local bandgap energies (ΔE/a.u.) and immobile charges induced by polarization discontinuity are simultaneously controlled throughout the structures, and optimized band profiles are eventually achieved for H@AlGaN, H@AlGaSiN, H@AlGaGeN, H@AlGaPdN,

and H@AlGaPtN. <S^2> has been ameliorated after doping the semiconductor atoms of silicon, germanium, and noble transition metals of palladium and platinum on the ternary AlGaN alloy, which might increase electron charge transfer in superconductor devices.

3.2. Analysis of nuclear quadrupole resonance spectra.

The NQR frequencies have been measured for AlGaSiN, AlGaGeN, AlGaPdN, and AlGaPtN towards estimating the hydrogenated nanoclusters of H@AlGaSiN, H@AlGaGeN, H@AlGaPdN, and H@AlGaPtN (Table 2). The NQR method is related to the multipole expansion in Cartesian coordinates as in equation (6) [57–62]:

$$V(r) = V(0) + \left[\left(\frac{\partial V}{\partial x_i}\right)\Big|_0 . x_i\right] + \frac{1}{2}\left[\left(\frac{\partial^2 V}{\partial x_i x_j}\right)\Big|_0 . x_i x_j\right] \quad (6)$$

$$U = -\frac{1}{2}\int_{\mathcal{D}} d^3 r\, \rho_r \left[\left(\frac{\partial^2 V}{\partial x_i^2}\right)\Big|_0 . x_i^2\right] = -\frac{1}{2}\int_{\mathcal{D}} d^3 r\, \rho_r \left[\left(\frac{\partial E_i}{\partial x_i}\right)\Big|_0 . x_i^2\right] = -\frac{1}{2}\left(\frac{\partial E_i}{\partial x_i}\right)\Big|_0 . \int_{\mathcal{D}} d^3 r\, [\rho(r) . x_i^2] \quad (7)$$

Table 2. Data of Bader charge (Q/Coulomb) and potential energy (E_p/a.u.) for AlGaSiN, H@AlGaSiN, AlGaGeN, H@AlGaGeN, AlGaPdN, H@AlGaPdN, AlGaPtN, and H@AlGaPtN hetero-clusters.

AlGaSiN			H@AlGaSiN			AlGaGeN			H@AlGaGeN		
Atom	**Q**	**E_p**	**Atom**	**Q**	**E_p**	**Atom**	**Q**	**E_p**	**Atom**	**Q**	**E_p**
Ga1	1.0145	–1.2293	Ga1	0.9919	–1.2418	Ga1	1.0106	–1.2310	Ga1	0.9784	-1.2470
N2	–1.1427	–18.3948	N2	–1.1462	–18.4011	N2	–1.1420	–18.3962	N2	–1.1475	-18.4047
Al3	1.2522	–1.2023	Al3	1.2832	–1.2007	Al3	1.2476	–1.2043	Al3	1.2976	-1.2024
N4	–1.1045	–18.4112	N4	–1.0695	–18.3870	N4	–1.0930	–18.4185	N4	–1.0819	-18.3962
Si5	0.7566	–1.8973	Si5	0.7501	–1.8495	Ge5	0.7604	–1.8300	Ge5	0.6899	-1.8020
Ga6	0.9752	–1.2344	Ga6	0.9583	–1.2420	Ga6	0.9708	–1.2364	Ga6	0.9852	-1.2364
N7	–1.1268	–18.3991	N7	–1.1213	–18.4082	N7	–1.1269	–18.4005	N7	–1.1483	-18.4017
Al8	1.2902	–1.1990	Al8	1.2802	–1.2115	Al8	1.2854	–1.2007	Al8	1.2668	-1.2103
N9	–1.1861	–18.4051	N9	–1.1838	–18.4157	N9	–1.1864	–18.4065	N9	–1.2073	-18.4157
N10	–0.7902	–18.4041	N10	–0.7725	–18.4174	N10	–0.7894	–18.4050	N10	–0.7707	-18.4142
Ga11	1.0153	–1.2386	Ga11	1.0639	–1.2317	Ga11	1.0092	–1.2406	Ga11	1.0702	-1.2337
N12	–1.1390	–18.3958	N12	–1.1318	–18.3903	N12	–1.1251	–18.4022	N12	–1.1185	-18.3988
Al13	1.1938	–1.2237	Al13	1.2028	–1.2280	Al13	1.1914	–1.2251	Al13	1.2308	-1.2200
N14	–0.7775	–18.4005	N14	–0.8328	–18.4281	N14	–0.7773	–18.4014	N14	–0.7833	-18.4186
Ga15	1.0280	–1.2408	Ga15	1.0092	–1.2441	Ga15	1.0223	–1.2428	Ga15	1.0407	-1.2385
N16	–0.6448	–18.3454	N16	–0.6320	–18.3565	N16	–0.6448	–18.3467	N16	–0.6289	-18.3568
N17	–0.6142	–18.3417	N17	–0.6327	–18.3549	N17	–0.6129	–18.3432	N17	–0.6330	-18.3548
			H18	–0.0174	–1.0120				H18	–0.0401	-1.0384
AlGaPdN			**H@AlGaPdN**			**AlGaPtN**			**H@AlGaPtN**		
Atom	**Q**	**E_p**	**Atom**	**Q**	**E_p**	**Atom**	**Q**	**E_p**	**Atom**	**Q**	**E_p**
Ga1	1.0197	–1.2296	Ga1	1.0144	–1.2281	Ga1	1.0296	–1.2264	Ga1	1.0120	–1.2306
N2	–1.1542	–18.3993	N2	–1.1640	–18.3900	N2	–1.1551	–18.3956	N2	–1.1543	–18.3964
Al3	1.2464	–1.2103	Al3	1.2954	–1.1935	Al3	1.2607	–1.2042	Al3	1.2596	–1.2012
N4	–0.8860	–18.3944	N4	–0.9111	–18.3861	N4	–0.9550	–18.3833	N4	–1.0208	–18.3769
Pd5	0.3351	–16.3098	Pd5	0.1988	–16.2830	Pt5	0.4083	–14.8314	Pt5	0.2914	–14.8045
Ga6	0.9649	–1.2440	Ga6	0.9996	–1.2295	Ga6	0.9764	–1.2381	Ga6	0.9953	–1.2327
N7	–1.1344	–18.4034	N7	–1.1330	–18.3955	N7	–1.1356	–18.3993	N7	–1.1495	–18.396
Al8	1.2922	–1.1996	Al8	1.3138	–1.1960	Al8	1.3086	–1.1963	Al8	1.2820	–1.1996
N9	–1.1921	–18.4049	N9	–1.1890	–18.403	N9	–1.1911	–18.4030	N9	–1.2098	–18.4017
N10	–0.8065	–18.4116	N10	–0.7750	–18.4130	N10	–0.8109	–18.4112	N10	–0.7700	–18.4067
Ga11	1.0388	–1.2424	Ga11	1.0760	–1.2289	Ga11	1.0590	–1.2374	Ga11	1.0862	–1.2273
N12	–0.9359	–18.3900	N12	–0.9211	–18.3801	N12	–1.0113	–18.3763	N12	–0.9789	–18.3696
Al13	1.2001	–1.2232	Al13	1.2236	–1.2161	Al13	1.2068	–1.2217	Al13	1.2564	–1.2058
N14	–0.7799	–18.4018	N14	–0.8321	–18.4186	N14	–0.7850	–18.401	N14	–0.7735	–18.4056
Ga15	1.0385	–1.2439	Ga15	1.0614	–1.2349	Ga15	1.0583	–1.2388	Ga15	1.0974	–1.2264
N16	–0.6380	–18.3426	N16	–0.6337	–18.3452	N16	–0.6441	–18.3438	N16	–0.6373	–18.3475
N17	–0.6087	–18.3426	N17	–0.6319	–18.3448	N17	–0.6196	–18.3423	N17	–0.6264	–18.3476
			H18	0.0080	–1.0864				H18	0.0402	–1.0880

The interaction of a nuclear quadrupole moment with the local inhomogeneous electric field removes the degeneracy of the nuclear ground state. The transition frequencies between

nuclear quadrupole energy levels, typically in the MHz range, depend on the nuclear quadrupole moment and the electric field gradient tensor at the nucleus. The "electric potential" through carrying over the electric charge was measured for AlGaSiN/ H@ AlGaSiN, AlGaGeN/H@AlGaGeN, AlGaPdN/H@AlGaPdN, AlGaPtN/H@AlGaPtN complexes (Table 2). Al, Ga, Si, Ge, Pd, Pt, N, and the hydrogen atom absorbed on AlGaN, AlGaSiN, AlGaGeN, AlGaPdN, and AlGaPtN have been calculated through the "Bader charge" and electronic potential properties. The elements of N2, N4, N7, N9, N10, N12, N14 of AlGaN, AlGaSiN, AlGaGeN, AlGaPdN, AlGaPtN have exhibited the most efficiency for admitting the electron from the "electron donor" of H18 adsorbed on AlGaN, AlGaSiN, AlGaGeN, AlGaPdN, AlGaPtN (Table 2).

In Figure 5 (a–d), the electric potential versus Bader charge for Al, Ga, Si, Ge, Pd, Pt, N, and the hydrogen atom absorbed on AlGaSiN, AlGaGeN, AlGaPdN, and AlGaPtN.

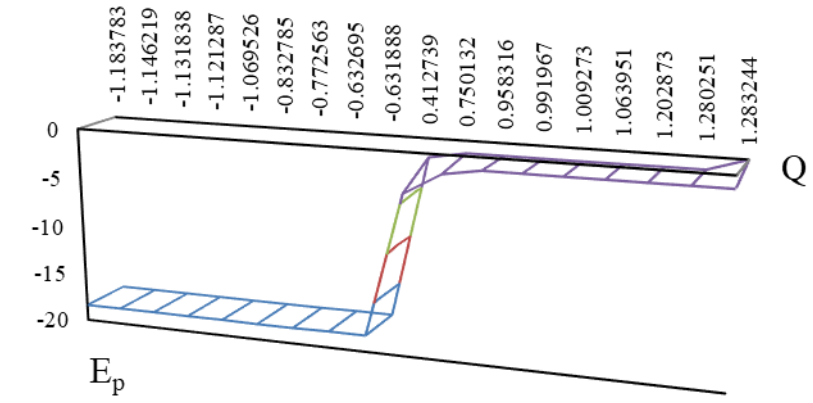

(a)

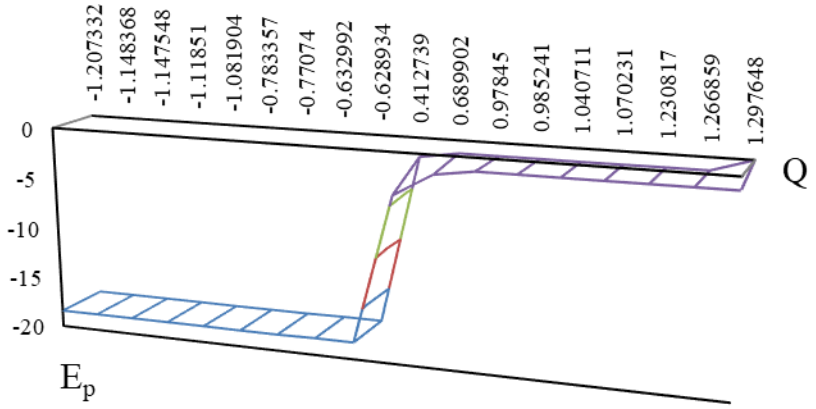

(b)

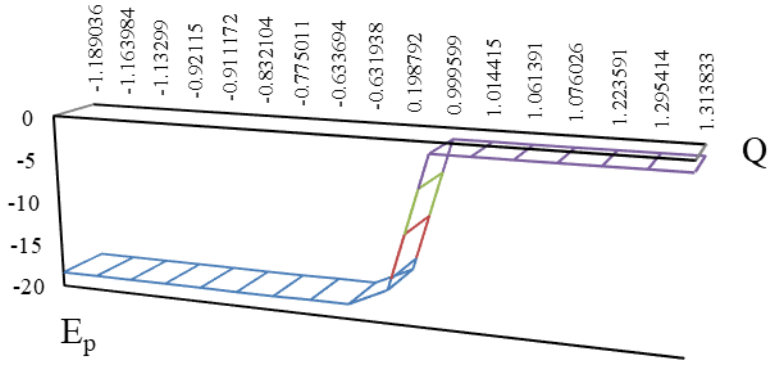

(c)

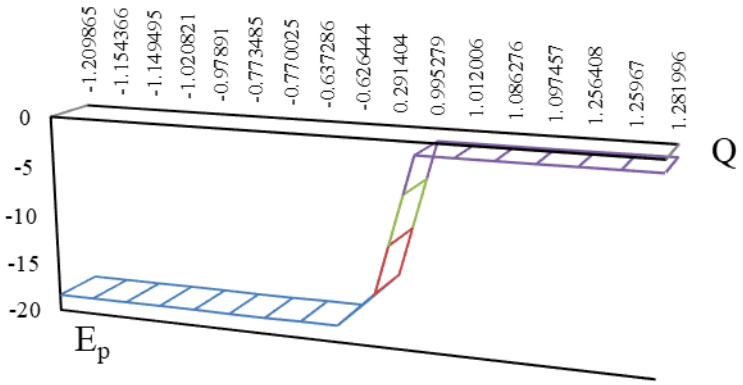

(d)

Figure 5. The graph of potential energy (E_p) versus atomic charge (Q) for **(a)** AlGaSiN/ H@AlGaSiN; **(b)** AlGaGeN/ H@AlGaGeN; **(c)** AlGaPdN/ H@AlGaPdN; **(d)** AlGaPtN/H@AlGaPtN heteroclusters.

It was observed that the similar behavior of hydrogen adsorption by AlGaSiN, AlGaGeN (Figure 5a,b), was characterized by high sensitivity based on the relation coefficient of $R^2 = 0.997$. Moreover, AlGaPdN and AlGaPtN have indicated similar behavior for hydrogen adsorption with a relation coefficient of about $R^2 = 0.998$ (Figure 5c,d).

The fluctuating peaks in the electric potential have been observed around hydrogen adsorption on AlGaSiN, AlGaGeN, AlGaPdN, and AlGaPtN, demonstrating the electron-accepting properties of hydrogen by Si, Ge, Pd, and Pt atoms (Figure 5a–d).

3.3. Insight into infrared spectroscopy and thermochemistry.

The infrared spectroscopy (IR) has been performed for the ternary nanocage of AlGaN (Figure 6a) and hybrid alloys of AlGaSiN (Figure 6b), AlGaGeN (Figure 6c), AlGaPdN (Figure 6d), and AlGaPtN (Figure 6e) through hydrogen adsorption.

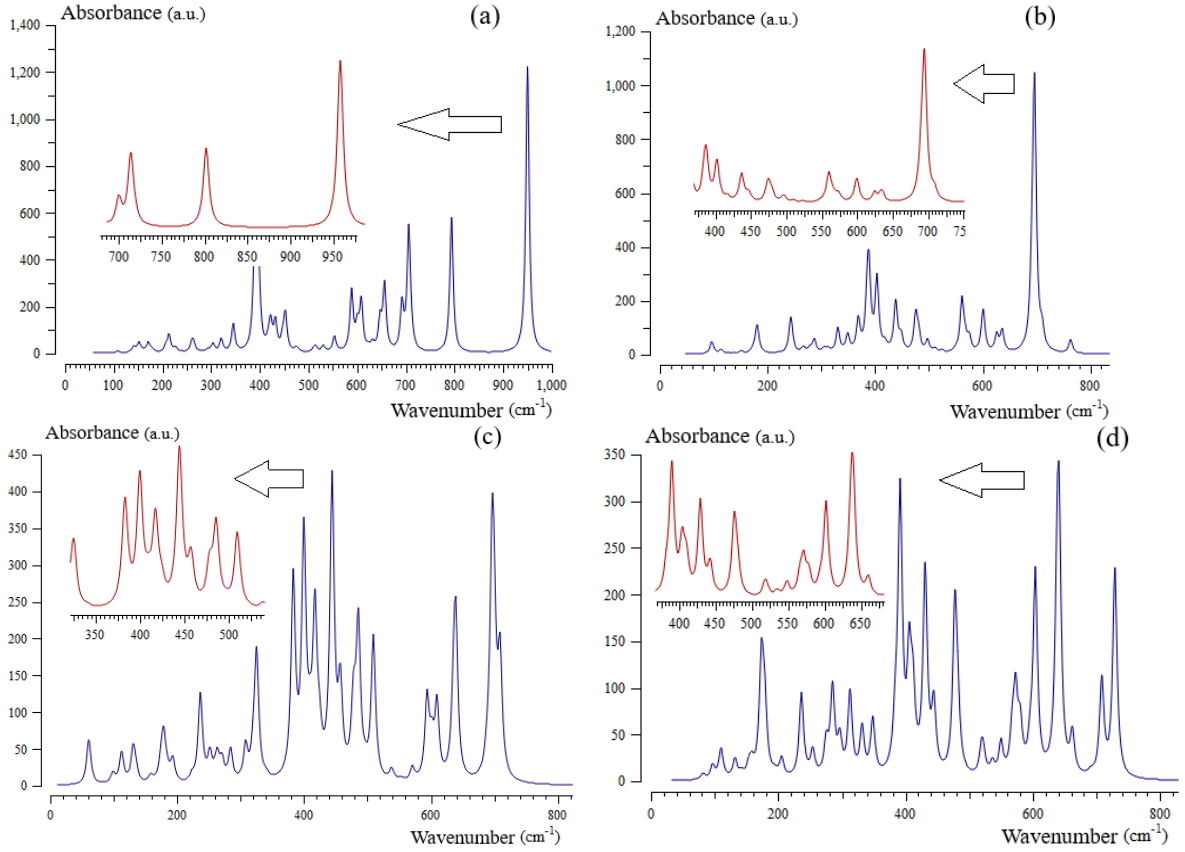

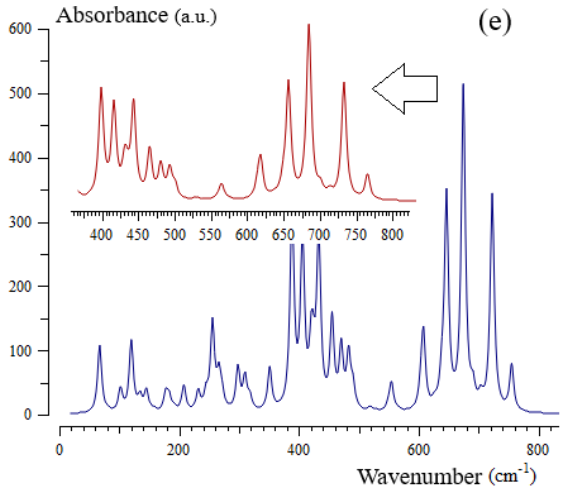

Figure 6. The wavenumber (cm^{-1}) changes through the IR spectra for hetero-clusters of **(a)** H@AlGaN; **(b)** H@AlGaSiN; **(c)** H@AlGaGeN; **(d)** H@AlGaPdN; **(e)** H@AlGaPtN.

The frequency values through the IR curves between 100–1000 cm^{-1} have been achieved for H@AlGaN with several sharp peaks around 396.73, 705.98,793.75, 941.91 cm^{-1} (Figure 6a). Figure 6 (b) shows the frequency range between 100–800 cm^{-1} for AlGaSiN –H with sharp peaks around 388.35, 403.32, and 606.23 cm^{-1}. Figure 6(c) indicates the fluctuation of frequency between 100–800 cm^{-1} for H@AlGaGeN with strong and sharp peaks around 399.71, 444.26, and 696.52 cm^{-1}. The graph of Figure 6(d) has been observed in the frequency range between 100–800 cm^{-1} for H@AlGaPdN with several sharp peaks around 391.43, 477.43, 641.08, and 728.76cm^{-1}. Furthermore, the graph of Figure 6(e) has been observed in the frequency range between 100–800 cm^{-1} for H@AlGaPtN with several sharp peaks around 405.90, 433.01, 646.34, 674.46, and 722.73 cm^{-1}.

Energy storage with heteroclusters has been described, where the frame of the overcoming cluster is related to AlGaPtN or AlGaPdN at high frequency. This property makes AlGaPtN or AlGaPdN potentially advantageous for certain high-frequency applications requiring transistor cells for energy storage. The advantages of platinum or palladium over aluminum gallium nitride include higher electron and hole mobilities, enabling platinum- or palladium-doped devices to operate at higher frequencies than silicon- or germanium-doped devices. Table 3, based on thermodynamic considerations, concluded that heteroclusters of AlGaN, AlGaSiN, AlGaGeN, AlGaPdN, or AlGaPtN might be a more efficient structure for energy storage in transistor cells.

Table 3. The thermodynamic characters of AlGaN/H@AlGaN, AlGaSiN/H@AlGaSiN, AlGaGeN/H@AlGaGeN, AlGaPdN/H@AlGaPdN, and AlGaPtN/H@AlGaPtN nanoclusters using CAM–B3LYP–D3/6-311+G(*d*, *p*) calculation.

Compound	Dipole moment (Debye)	$\Delta E^{o}_{ads} \times 10^{-3}$ (kcal/mol)	$\Delta H^{o}_{ads} \times 10^{-3}$ (kcal/mol)	$\Delta G^{o}_{ads} \times 10^{-3}$ (kcal/mol)	E^{o} H@$_{binding}$ (kcal/mol)
AlGaN	4.6672	–319.178	–319.178	–319.219	-
H@AlGaN	5.5817	–319.503	–319.502	–319.542	–325
AlGaSiN	5.8081	–320.296	–320.295	–320.335	-
H@AlGaSiN	5.0608	–320.656	–320.656	–320.697	–360
AlGaGeN	5.6442	–320.240	–320.239	–320.279	-
H@AlGaGeN	4.3890	–320.608	–320.607	–320.650	–368
AlGaPdN	5.1550	–397.327	–397.327	–397.368	-
H@AlGaPdN	6.2464	–397.686	–397.686	–397.729	–359
AlGaPtN	5.5186	–392.573	–392.573	–392.614	-
H@AlGaPtN	5.0840	–392.956	–392.956	–392.999	–383

Thermodynamic parameters of hetero-clusters of AlGaN/H@AlGaN, AlGaSiN/H@AlGaSiN, AlGaGeN/H@AlGaGeN, AlGaPdN/H@AlGaPdN, and AlGaPtN/H@AlGaPtN have been assigned (Table 3). The changes of Gibbs free energy versus dipole moment could detect the maximum efficiency of H@AlGaPdN and H@AlGaPtN hetero-clusters for energy storage in the transistor cells through ΔG^{o}_{ads} (Table 3).

The adsorption efficiency of H@AlGaN, H@AlGaSiN, H@AlGaGeN, H@AlGaPdN, and H@AlGaPtN based on dipole moment has been evaluated by the ΔG^{o}_{ads}. The transistor cells formed by AlGaN, AlGaSiN, AlGaGeN, AlGaPdN, and AlGaPtN feature a hierarchical structure with the electron donor/acceptor layer sandwiched between the anode and cathode, which underscores the importance of controlling the molecular crystal orientation, domain size, and vertical distribution to facilitate charge collection at the electrodes. In this paper, we have demonstrated that the ternary semiconductor aluminum gallium nitride can lead to a significant absorption enhancement across a broad spectral range of incident light in the presence of silicon, germanium, palladium, or platinum. A comparison between transistor cells containing 4d and 5d transition metals, Pd and Pt, respectively, doped AlGaN shows that cells containing these elements exhibit enhanced cell performance compared to cells containing only the bare AlGaN structure. This efficient doping strategy not only bridges the gaps in heteroatom-doped AlGaN-based semiconductor materials but also provides deep insights into controlling the electrical and optical properties of these hybrid nanocluster dopants.

4. Conclusions

In summary, hydrogen grabbing on the hetero-clusters of AlGaN, AlGaSiN, AlGaGeN, AlGaPdN, and AlGaPtN as transistor cells was investigated by first-principles calculations. We have provided a ternary aluminum gallium nitride solar cell doped with silicon, germanium, palladium, or platinum. The geometrical parameters of doping atoms on the surface of AlGaN were studied using the absorption status and current charge density of the transistor cells. Moreover, the effect of a relative chemical shift between AlGaN and doped heteroclusters of the transistor cell was also investigated. Thermodynamic parameters have constructed a detailed molecular model for atom–atom interactions and a distribution of point charges which can be utilized to reproduce the polarity of the solid material and the adsorbing molecules. Energy storage with heteroclusters has been described, where the frame of the overcoming cluster is related to AlGaPdN or AlGaPtN at high frequency. This property makes AlGaPdN or AlGaPtN potentially advantageous for certain high-frequency applications requiring transistor cells for energy storage due to hydrogen adsorption by formation of H@AlGaN, H@AlGaSiN, H@AlGaGeN, H@AlGaPdN, or H@AlGaPtN. The advantages of platinum or palladium over aluminum gallium nitride include higher electron and hole mobilities, enabling platinum- or palladium-doped devices to operate at higher frequencies than silicon- or germanium-doped devices. Thus, it should be explored for its unique properties, such as its ability to increase energy storage, which could lead to advancements in transistor cells.

Institutional Review Board Statement

Not applicable.

Informed Consent Statement

Not applicable.

Data Availability Statement

Not applicable.

Funding

This research received no external funding.

Acknowledgments

The author is grateful to Kastamonu University for successfully completing this paper and its research.

Conflict of Interest

The author declares no conflict of interest.

References

1. Mollaamin, F.; Monajjemi, M. Structural, Electromagnetic and Thermodynamic Analysis of Ion Pollutants Adsorption in Water by Gallium Nitride Nanomaterial: a Green Chemistry Application. *Russ. J. Phys. Chem. B* **2024**, *18*, 533–548, https://doi.org/10.1134/S199079312402012X.
2. Mollaamin, F.; Monajjemi, M. Determination of GaN nanosensor for scavenging of toxic heavy metal ions (Mn^{2+}, Zn^{2+}, Ag^{+}, Au^{3+}, Al^{3+}, Sn^{2+}) from water: Application of green sustainable materials by molecular modeling approach. *Comput. Theor. Chem.* **2024**, *1237*, 114646, https://doi.org/10.1016/j.comptc.2024.114646.
3. Sun, J.; Sun, Y.; Wu, D.; Cai, Y.; Qin, H.; Zhang, B. High-responsivity, low-noise, room-temperature, self-mixing terahertz detector realized using floating antennas on a GaN-based field-effect transistor. *Appl. Phys. Lett.* **2012**, *100*, 013506, https://doi.org/10.1063/1.3673617.
4. Mollaamin, F.; Monajjemi, M. The influence of Sc, V, Cr, Co, Cu, Zn as ferromagnetic semiconductors implanted on B_5N_{10}-nanocarrier for enhancing of NO sensing: An environmental eco-friendly investigation. *Comput. Theor. Chem*. **2024**, *1237*, 114666, https://doi.org/10.1016/j.comptc.2024.114666.
5. Mollaamin, F.; Monajjemi, M. Trapping of toxic heavy metals from water by GN–nanocage: Application of nanomaterials for contaminant removal technique. *J. Mol. Struct.* **2024**, *1300*, 137214, https://doi.org/10.1016/j.molstruc.2023.137214.
6. Mollaamin, F.; Monajjemi, M. Doping Effects in Ternary Aluminum Gallium Nitride Hetero-Cluster Towards High-Electron-Mobility Transistors for Hydrogen Sensing: A Density Functional Theory Study and Energy-Saving. *Russ. J. Phys. Chem. B* **2025**, *19*, 236–254, https://doi.org/10.1134/S1990793124701689.
7. Mollaamin, F.; Monajjemi, M. Unraveling Hetero-Clusters of Indium Gallium Nitride and Its Alloys for Solar Cells Development: Structural and Characterization Study of Nitride-Based Semiconductors Using DFT Framework. *Russ. J. Phys. Chem. B* **2025**, *19*, 480–500, https://doi.org/10.1134/S1990793125700174.
8. Belhachi, S.; Merabet, B.; Al-Qaisi, S.; Goumri-Said, S. Exploring the Multifunctional Properties of Tm-Doped $Al_xGa_{1-x}N$ Alloys: From Potoluminescence to Spintronics. *Int. J. Quantum Chem.* **2024**, *124*, e27520, https://doi.org/10.1002/qua.27520.
9. Belhachi, S. Stability, Electronic and Magnetic Properties of Rare Earth (Eu, Tm) Implanted InGaN. *J. Supercond. Nov. Magn.* **2019**, *32*, 2515–2519, https://doi.org/10.1007/s10948-018-4976-1.
10. Belhachi, S. Semiconductor Characteristic and Ferromagnetism in Rare Earth (Eu, Er)-Doped AlGaN Alloy: LSDA + U Approach. *Braz. J. Phys.* **2023**, *53*, 34, https://doi.org/10.1007/s13538-022-01249-7.
11. Mollaamin, F.; Monajjemi, M. Divulge of Hydrogen Energy Storage by Manganese Doped Nitrogen Nanocomposites of Aluminum, Gallium or Indium Nitrides: A First-Principles Study. *Russ. J. Phys. Chem. B.* **2025**, *19*, 319–335, https://doi.org/10.1134/S199079312570006X.
12. Blasco, R.; Ajay, A.; Robin, E.; Bougerol, C.; Lorentz, K.; Alves, L.; Mouton, I.; Amichi, L.; Grenier, A.; Monroy, E. Electrical and optical properties of heavily Ge-doped AlGaN. *J. Phys. D: Appl. Phys.* **2019**, *52*, 125101, https://doi.org/10.1088/1361-6463/aafec2.

13. Lien, D.-H.; Hsiao, Y.-H.; Yang, S.-G.; Tsai, M.-L.; Wei, T.-C.; Lee, S.-C.; He, J.-H. Harsh photovoltaics using InGaN/GaN multiple quantum well schemes. *Nano Energy* **2015**, *11*, 104-109, https://doi.org/10.1016/j.nanoen.2014.10.013.
14. Mollaamin, F. Stating the Progress of Mn-Based Nanohybrid Materials Containing GaN/AlGaN/InGaN Towards Remarkable Improvement in Hydrogen Storage. *Nanosistemi, Nanomateriali, Nanotehnologii* **2025**, *23*, 37–60, https://doi.org/10.15407/nnn.23.01.0037.
15. Young, N.; Farrell, R.; Hu, Y.; Terao, Y.; Iza, M.; Keller, S.; DenBaars, S.; Nakamura, S.; Speck, J. High performance thin quantum barrier InGaN/GaN solar cells on sapphire and bulk (0001) GaN substrates. *Appl. Phys. Lett.* **2013**, *103*, https://doi.org/10.1063/1.4826483.
16. Mollaamin, F. Evaluation of selectivity and sensitivity of gallium nitride nanosensor for grabbing metal/ metalloid ions (Na^+, K^+, Sn^{2+}, Pb^{2+}, Al^{3+}) from water: materials modelling approach towards environmental treatment. *Functional Materials* **2025**, *32*, 306–314. http://dx.doi.org/10.15407/fm32.02.306
17. Mollaamin, F.; Monajjemi, M. Application of DFT and TD-DFT on Langmuir Adsorption of Nitrogen and Sulfur Heterocycle Dopants on an Aluminum Surface Decorated with Magnesium and Silicon. *Computation* **2023**, *11*, 108, https://doi.org/10.3390/computation11060108.
18. Shahriari, S.; Mollaamin, F.; Monajjemi, M. Increasing the Performance of {[(1-x-y) $LiCo_{0.3}Cu_{0.7}$] (Al and Mg doped)] O_2}, xLi_2MnO_3, $yLiCoO_2$ Composites as Cathode Material in Lithium-Ion Battery: Synthesis and Characterization. *Micromachines* **2023**, *14*, 241, https://doi.org/10.3390/mi14020241.
19. Mollaamin, F.; Shahriari, S.; Monajjemi, M. Influence of Transition Metals for Emergence of Energy Storage in Fuel Cells through Hydrogen Adsorption on the MgAl Surface. *Russ. J. Phys. Chem. B.* **2024**, *18*, 398–418, https://doi.org/10.1134/S199079312402026X.
20. Mollaamin, F.; Shahriari, S.; Monajjemi, M.; Khalaj, Z. Nanocluster of Aluminum lattice via organic inhibitors coating: A study of freundlich adsorption. *J. Clust. Sci.* **2023**, *34*, 1547–1562, https://doi.org/10.1007/s10876-022-02335-1.
21. Chriki, R.; Yanai, A.; Shappir, J.; Levy, U. Enhanced efficiency of thin film solar cells using a shifted dual grating plasmonic structure. *Opt Express* **2013**, *21*, A382-A391, https://doi.org/10.1364/OE.21.00A382.
22. Mollaamin, F. Alkali Metals Doped on Tin-Silicon and Germanium-Silicon Oxides for Energy Storage in Hybrid Biofuel Cells: A First-Principles Study. *Russ. J. Phys. Chem. B.* **2025**, *19*, 722–736, https://doi.org/10.1134/S1990793125700393.
23. Mollaamin, F.; Monajjemi, M. Electric and Magnetic Evaluation of Aluminum–Magnesium Nanoalloy Decorated with Germanium Through Heterocyclic Carbenes Adsorption: A Density Functional Theory Study. *Russ. J. Phys. Chem. B.* **2023**, *17*, 658–672, https://doi.org/10.1134/S1990793123030223.
24. Lin, J.; Yu, Y.; Xu, Z.; Gao, F.; Zhang, Z.; Zeng, F.; Wang, W.; Li, G.; Electronic engineering of transition metal Zn-doped InGaN nanorods arrays for photoelectrochemical water splitting. *J. Power Sources* **2020**, *450*, 227578, https://doi.org/10.1016/j.jpowsour.2019.227578.
25. Kumawat, U.K.; Kumar, K.; Bhardwaj, P.; Dhawan, A. Indium-rich InGaN/GaN solar cells with improved performance due to plasmonic and dielectric nanogratings. *Energy Sci. Eng.* **2019**, *7*, 2469-2482, https://doi.org/10.1002/ese3.436.
26. Zainal, N.; Hagedorn, S.; Netzel, C.; Kolbe, T.; Weyers, M. High-Temperature Annealing of Si-Doped AlGaN. *Phys. Status Solidi A* **2024**, *221*, 2300897, https://doi.org/10.1002/pssa.202300897.
27. Mollaamin, F.; Monajjemi, M. Application of Smart Condensed H-Adsorption Nanocomposites in Batteries: Energy Storage Systems and DFT Computations. *Computation* **2024**, *12*, 234. https://doi.org/10.3390/computation12120234.
28. Mollaamin, F. Investigating the Treatment of Transition Metals for Ameliorating the Ability of Boron Nitride for Gas Sensing & Removing: A Molecular Characterization by DFT Framework. *Prot. Met. Phys. Chem. Surf.* **2024**, *60*,1050–1063, https://doi.org/10.1134/S2070205124702502.
29. Mollaamin, F.; Monajjemi, M. Perspective of Clean Energy-saving by Semiconducting Quantum Dot Nanomaterials through Photoelectric and Density of States Analysis. *J Fluoresc.* **2025**, https://doi.org/10.1007/s10895-025-04207-z.
30. Akhtar, M.; Alanazi, F.K.; Sajid, M.; Abdalla, S.; Belhachi, S.; Nazar, M.; Murtaza, S.; Naqvi, S.M.K.A.; Alqorashi, A.K.; Alawaideh, Y.M. Investigating the Physical Characteristics of Halide Double Perovskites X_2LiSbI_6 (X= K, Cs): A First-Principles Approach. *J. Inorg. Organomet. Polym. Mater.* **2025**, 35, 4810-4824, https://doi.org/10.1007/s10904-024-03560-z.
31. Riaz, K.; Drissi, N.; Abdalla, S.; Belhachi, S.; Bousbih, R.; Soliman, M.S.; Nasarullah; Hasanin, T.H.; Nazar, M.; Abdulhussein, N.A. Computational Exploration of Structural, Elastic, Optoelectronic and

Magnetic Properties of A_2YHgCl_6 (A= Cs, K) Using Enhanced Computational Techniques. *J. Inorg. Organomet. Polym. Mater.* **2025**, *35*, 5363-5376, https://doi.org/10.1007/s10904-025-03594-x.

32. Ullah, A.; Rahman, N.; Husain, M.; Abualnaja, K.M.; Alosaimi, G.; Belhachi, S.; Al-Khamiseh, B.M.; Tirth, V.; Azzouz-Rached, A.; Althobaiti, H.A. Unlocking the physical properties of RbXBr3 (X= Ba, Be) halide perovskites for potential applications: DFT study. *Inorg. Chem. Commun.* **2025**, *173*, 113879, https://doi.org/10.1016/j.inoche.2024.113879.
33. Ullah, W.; Rahman, N.; Husain, M.; Almalki, W.M.; Abualnaja, K.M.; Alosaimi, G.; Belhachi, S.; Al-Khamiseh, B.M.; Tirth, V.; Azzouz-Rached, A. Modelling of structural, mechanical, electronic, and optical properties of Rb2TlXF6 (X= Ir, Rh) double perovskite compounds through density functional theory. *Results Phys.* **2025**, *68*, 108079, https://doi.org/10.1016/j.rinp.2024.108079.
34. Rahman, N.; Azzouz-Rached, A.; Husain, M. Correction: Impact of samarium on magnetic and optoelectronic properties of magnesium-based MgSm2X4 (X = S and Se) spinels for spintronics. *PLoS ONE.* **2024**, *19*, e0309388, https://doi.org/10.1371/journal.pone.0309388.
35. Rahman, N.; Abualnaja, K.M.; Belhachi, S.; Sfina, N.; Husain, M.; Al-Khamiseh, B.M.; Azzouz-Rached, A.; Althobaiti, H.A.; Ullah, S.; Khan, R. DFT insights on the future prospects of Ba_2PrXO_6 (X= Ir, Pt) double perovskites for high-energy applications. *J. Inorg. Organomet. Polym. Mater.* **2025**, *35*, 1439-1452, https://doi.org/10.1007/s10904-024-03363-2.
36. Belhachi, S.; Al-Qaisi, S.; Samah, S.; Rached, H.; Zaman, A.; Alrebdi, T.A.; Boutramine, A.; Erum, N.; Ahmed, R.; Verma, A.S. DFT analysis of Ba2NbRhO6: a promising double perovskite for sustainable energy applications. *J. Inorg. Organomet. Polym. Mater.* **2025**, *35*, 978-993, https://doi.org/10.1007/s10904-024-03336-5.
37. Sfina, N.; Rahman, N.; Belhachi, S.; Husain, M.; Al-Khamiseh, B.M.; Abualnaja, K.M.; Alosaimi, G.; Azzouz-Rached, A.; Ullah, S.; Rashid, A.U. Exploring novel Ba2MBiO6 (M= Sm, Tb) oxide double perovskites employing DFT. *J. Inorg. Organomet. Polym. Mater.* **2024**, *34*, 6102-6113, https://doi.org/10.1007/s10904-024-03242-w.
38. Belhachi, S.; Kanoun, M.B.; Goumri-Said, S. Unveiling the potential of $CuAl_xGa1{-}xSe_2$ (x = 0.25) chalcopyrite as absorbent for photovoltaic application: first-principles insights into the structural, elastic, mechanical, electronic, thermodynamic and optical properties. *Phys. Scr.* **2024**, *99*, 085921, https://doi.org/10.1088/1402-4896/ad5b93.
39. Boutramine, A.; Al-Qaisi, S.; Samah, S.; Iram, N.; Alrebdi, T.A.; Bouzgarrou, S.; Verma, A.S.; Belhachi, S.; Sharma, R. Optoelectronic and thermoelectric properties of new lead-free K2NaSbZ6 (Z= Br, I) halide double-perovskites for clean energy applications: a DFT study. *Opt. Quantum Electron.* **2024**, *56*, 417, https://doi.org/10.1007/s11082-024-06344-4.
40. Mollaamin, F. Competitive Intracellular Hydrogen-Nanocarrier Among Aluminum, Carbon, or Silicon Implantation: a Novel Technology of Eco-Friendly Energy Storage using Research Density Functional Theory. *Russ. J. Phys. Chem. B.* **2024**, *18*, 805–820, https://doi.org/10.1134/S1990793124700131.
41. Belhachi, S. The effect of d and f states of ytterbium on the electronic and magnetic properties of Al1−xYbxN: DFT+U study. *Int. J. Mod. Phys. B* **2018**, *32*, 1850119, https://doi.org/10.1142/S0217979218501199.
42. Belhachi, S. Electronic and Magnetic Properties of $Ru_2FeSi_{1-x}Ge_x$ Alloys in B2 Structure: a First-Principle Study. *J. Supercond. Nov. Magn.* **2018**, *31*, 1155–1159, https://doi.org/10.1007/s10948-017-4291-2.
43. Frisch, M.J.; Trucks, G.W.; Schlegel, H.B.; Scuseria, G.E.; Robb, M.A.; Cheeseman, J.R.; Scalmani, G.; Barone, V.; Petersson, G.A.; Nakatsuji, H.; Li, X.; Caricato, M.; Marenich, A.V.; Bloino, J.; Janesko, B.G.; Gomperts, R.; Mennucci, B.; Hratchian, H.P.; Ortiz, J. V.; Izmaylov, A. F.; Sonnenberg, J.L.; Williams-Young, D.; Ding, F.; Lipparini, F.; Egidi, F.; Goings, J.; Peng, B.; Petrone, A.; Henderson, T.; Ranasinghe, D.; Zakrzewski, V.G.; Gao, J.; Rega, N.; Zheng, G.; Liang, W.; Hada, M.; Ehara, M.; Toyota, K.; Fukuda, R.; Hasegawa, J.; Ishida, M.; Nakajima, T.; Honda, Y.; Kitao, O.; Nakai, H.; Vreven, T.; Throssell, K.; Montgomery, J.A., Jr.; Peralta, J.E.; Ogliaro, F.; Bearpark, M.J.; Heyd, J.J.; Brothers, E.N.; Kudin, K.N.; Staroverov, V.N.; Keith, T.A.; Kobayashi, R.; Normand, J.; Raghavachari, K.; Rendell, A.P.; Burant, J.C.; Iyengar, S.S.; Tomasi, J.; Cossi, M.; Millam, J.M.; Klene, M.; Adamo, C.; Cammi, R.; Ochterski, J.W.; Martin, R.L.; Morokuma, K.; Farkas, O.; Foresman, J.B.; Fox, D.J. Gaussian 16, Revision C.01, Gaussian, Inc., Wallingford CT, **2016**.
44. Dennington, R.; Keith Todd, A.; Millam John, M. GaussView, Version 6.06.16. Semichem Inc., Shawnee Mission, KS, USA, **2016**.

45. Lee, C.; Yang, W.; Parr, R.G. Development of the Colle–Salvetti correlation-energy formula into a functional of the electron density. *Phys. Rev. B* **1988**, *37*, 785–789, https://doi.org/10.1103/physrevb.37.785.
46. Mollaamin, F.; Monajjemi, M. An Architectural Battery Designed by Substituting Lithium with Second Main Group Metals (Be, Mg, Ca/Cathode) and Hybrid Oxide of Fourth Group Ones (Si, Ge, Sn/Anode) Nanomaterials Towards H_2 Adsorption: A Computational Study. *Nanomaterials* **2025**, *15*, 959, https://doi.org/10.3390/nano15130959
47. Grimme, S.; Antony, J.; Ehrlich, S.; Krieg, H. A consistent and accurate ab initio parametrization of density functional dispersion correction (DFT-D) for the 94 elements H-Pu. *J. Chem. Phys*. **2010**, *132*, 154104, https://doi.org/10.1063/1.3382344.
48. Salikhov, K.M., Zavoiskaya, N.E. Zavoisky and the discovery of EPR. *Resonance* **2015**, *20*, 963–968, https://doi.org/10.1007/s12045-015-0264-6.
49. Xu, Z.; Qin, C.; Yu, Y.; Jiang, G.; Zhao, L. First-principles study of adsorption, dissociation, and diffusion of hydrogen on α-U (110) surface. *AIP Adv.* **2024**, *14*, 055114, https://doi.org/10.1063/5.0208082.
50. Mollaamin, F.; Monajjemi, M. Adsorption ability of Ga_5N_{10} nanomaterial for removing metal ions contamination from drinking water by DFT. *Int. J. Quantum Chem.* **2024**, *124*, e27348, https://doi.org/10.1002/qua.27348.
51. Mollaamin, F.; Monajjemi, M. Graphene-based resistant sensor decorated with Mn, Co, Cu for nitric oxide detection: Langmuir adsorption & DFT method. *Sensor Review* **2023**, *43*, 266–279, https://doi.org/10.1108/sr-03-2023-0040.
52. Matta, C.F.; Ayers, P.W.; Cook, R. The Physics of Electron Localization and Delocalization. In Electron Localization-Delocalization Matrices, Matta, C.F., Ayers, P.W., Cook, R., Eds.; Springer International Publishing: Cham, **2024**; pp. 7-20, https://doi.org/10.1007/978-3-031-51434-0_2.
53. Tian, L.; Chen, F.-W. Meaning and Functional Form of the Electron Localization Function. *Acta Phys. Chim. Sin*. **2011**, *27*, 2786–2792, https://doi.org/10.3866/PKU.WHXB20112786.
54. Mollaamin, F.; Monajjemi, M. Doping of Graphene Nanostructure with Iron, Nickel and Zinc as Selective Detector for the Toxic Gas Removal: A Density Functional Theory Study. *C* **2023**, *9*, 20, https://doi.org/10.3390/c9010020.
55. Lu, T.; Chen, F. Multiwfn: a multifunctional wavefunction analyzer. *J. Comput. Chem.* **2011**, *33*, 580–592, https://doi.org/10.1002/jcc.22885.
56. Lu, T. A comprehensive electron wavefunction analysis toolbox for chemists, Multiwfn. *J. Chem. Phys*. **2024**, *161*, 082503, https://doi.org/10.1063/5.0216272.
57. Mollaamin, F. Anchoring of 2D layered materials of $Ge_5Si_5O_{20}$ for (Li/Na/K)-(Rb/Cs) batteries towards Eco-friendly energy storage. *BMC Chemistry*. **2025**, *19*, 233, https://doi.org/10.1186/s13065-025-01593-0.
58. Mollaamin, F.; Monajjemi, M. In Silico-DFT Investigation of Nanocluster Alloys of Al-(Mg, Ge, Sn) Coated by Nitrogen Heterocyclic Carbenes as Corrosion Inhibitors. *J. Clust. Sci.* **2023**, *34*, 2901–2918, https://doi.org/10.1007/s10876-023-02436-5.
59. Trontelj, Z.; Pirnat, J.; Jazbinšek, V.; Lužnik, J.; Srčič, S.; Lavrič, Z.; Beguš, S.; Apih, T.; Žagar, V.; Seliger, J. Nuclear Quadrupole Resonance (NQR)–A Useful Spectroscopic Tool in Pharmacy for the Study of Polymorphism. *Crystals* **2020**, *10*, 450, https://doi.org/10.3390/cryst10060450.
60. Sciotto, R.; Ruiz Alvarado, I.A.; Schmidt, W.G. Substrate Doping and Defect Influence on P-Rich InP(001):H Surface Properties. *Surfaces* **2024**, *7*, 79–87, https://doi.org/10.3390/surfaces7010006.
61. Luo, J.; Wang, C.; Wang, Z.; Guo, Q.; Yang, J.; Rui Zhou, R.; Matano, K.; Oguchi, T.; Ren, Z. NMR and NQR studies on transition-metal arsenide superconductors $LaRu_2As_2$, $KCa_2Fe_4As_4F_2$, and $A_2Cr_3As_3$*. *Chinese Phys. B* **2020**, *29*, 067402, https://doi.org/10.1088/1674-1056/ab892d.
62. Mollaamin, F.; Monajjemi, M. Tailoring and functionalizing the graphitic-like GaN and GaP nanostructures as selective sensors for NO, NO_2, and NH_3 adsorbing: a DFT study. *J. Mol. Model.* **2023**, *29*, 170, https://doi.org/10.1007/s00894-023-05567-8.

Publisher's Note & Disclaimer